HHS Public Access

Author manuscript

J Mol Biol. Author manuscript; available in PMC 2017 August 19.

Published in final edited form as:

J Mol Biol. 2017 March 24; 429(6): 900–910. doi:10.1016/j.jmb.2017.02.005.

Dynamic Phenylalanine Clamp Interactions Define Single-Channel Polypeptide Translocation through the Anthrax Toxin Protective Antigen Channel

Koyel Ghosal[1], **Jennifer M. Colby**[2], **Debasis Das**[1], **Stephen T. Joy**[3], **Paramjit S. Arora**[3], and **Bryan A. Krantz**[1]

[1]Department of Microbial Pathogenesis, School of Dentistry, University of Maryland, Baltimore, 650 W, Baltimore Street, Baltimore, MD 21201, USA

[2]Department of Pathology, Microbiology and Immunology, Vanderbilt University School of Medicine, Nashville, TN 37232, USA

[3]Department of Chemistry, New York University, New York, NY 10003, USA

Abstract

Anthrax toxin is an intracellularly acting toxin where sufficient detail is known about the structure of its channel, allowing for molecular investigations of translocation. The toxin is composed of three proteins, protective antigen (PA), lethal factor (LF), and edema factor (EF). The toxin's translocon, PA, translocates the large enzymes, LF and EF, across the endosomal membrane into the host cell's cytosol. Polypeptide clamps located throughout the PA channel catalyze the translocation of LF and EF. Here, we show that the central peptide clamp, the ϕ clamp, is a dynamic site that governs the overall peptide translocation pathway. Single-channel translocations of a 10-residue, guest–host peptide revealed that there were four states when peptide interacted with the channel. Two of the states had intermediate conductances of 10% and 50% of full conductance. With aromatic guest–host peptides, the 50% conducting intermediate oscillated with the fully blocked state. A Trp guest–host peptide was studied by manipulating its stereochemistry and prenucleating helix formation with a covalent linkage in the place of a hydrogen bond or hydrogen-bond surrogate (HBS). The Trp peptide synthesized with L-amino acids translocated more efficiently than peptides synthesized with D- or alternating D,L-amino acids. HBS stapled Trp peptide exhibited signs of steric hindrance and difficulty translocating. However, when mutant ϕ clamp (F427A) channels were tested, the HBS peptide translocated normally. Overall, peptide translocation is defined by dynamic interactions between the peptide and ϕ clamp. These dynamics require conformational flexibility, such that the peptide productively forms both extended-chain and helical states during translocation.

Keywords

Bacillus anthracis; anthrax toxin; protective antigen; electrophysiology; peptide clamp

Correspondence to Bryan A. Krantz: bkrantz@umaryland.edu.

Introduction

Membranes form hydrophobic barriers that separate aqueous compartments in cells, requiring membrane-embedded transporters and channels to allow for movement of biomolecules across these barriers. Some of the largest cargos to be delivered across membranes include multidomain folded proteins. Many bacterial toxins possess their own translocase channel, which can deliver a cytotoxic enzyme across a membrane into the cytosol of the host cell. For example, anthrax toxin [1,2] is made up of three proteins, protective antigen (PA; 83 kDa), lethal factor (LF; 90 kDa), and edema factor (EF; 89 kDa). The PA component self-assembles into a ring-shaped oligomer that inserts into the lipid bilayer to make a translocase channel; LF and EF translocate through the channel into the cytosol.

In order for anthrax toxin to properly function, it must first self-assemble. PA initially binds to a host cell receptor and is cleaved by a furin-like protease. A small 20-kDa portion of PA dissociates, leaving the remaining 63 kDa to self-assemble into a ring-shaped heptamer [3] or octamer [4]. This oligomer is called the prechannel. As the oligomer assembles, it presents binding sites for LF and EF [5,6]. The assembled complexes are endocytosed. Once the endosome matures and its pH becomes more acidic, PA transforms from the prechannel state to the channel state [7]. The proton gradient established across the endosomal membrane drives LF and EF to unfold [8,9] and translocate [10] through the PA channel. Once in the cytosol, LF and EF refold and carry out their respective catalytic functions to disrupt cell signaling pathways. LF is a zinc metalloprotease that cleaves mitogen-activated protein kinase kinases [11], and EF is an adenylate cyclase [12].

LF and EF unfolding are required because the PA channel is so narrow that only structure as wide as an α helix can be sterically accommodated in most parts of the channel [9]. Substrate unfolding and translocation are catalyzed by a series of polypeptide clamp active sites that line the channel [2]. On the topmost surface of the channel is the α helix binding clamp (α clamp), which is a deep cleft between PA subunits that can bind to α helical structure. Within the channel is a ring of phenylalanine residues, called the phenylalanine clamp (ϕ clamp) [13], and this structure narrows considerably further to an opening of ~6 Å [14]—a diameter too narrow for α helical structure. The measured diameter of the channel was at pH 5.0, and no LF or EF was bound to that structure. The ϕ clamp, essential for translocation, preferentially binds to hydrophobic and aromatic functional groups [13], and it helps catalyze the unfolding step of translocation [8]. Beneath the ϕ clamp is a highly charged β barrel, called the charge clamp, which is required to harness the proton gradient driving force [15]. The charge clamp is highly anionic at the juncture nearest to the ϕ clamp.

Different models have been put forth on how proteins translocate through the PA channel. The extended-chain Brownian-ratchet model, on one hand, suggests that the translocating chain is in the fully extended conformation during translocation [16]. Carboxylates in the translocating chain are protonated on the low pH side of the membrane. Under Brownian motion, these protonated sites then diffuse past the charge clamp, which normally repels anionic groups, and then, the protonated residues deprotonate down the gradient, leaving them electrostatically committed to translocate toward the high pH side of the membrane.

The cycle repeats until the entire protein is translocated. In this proposed mechanism, the clamp sites in the channel are largely static structures.

The helix-compression model, on the other hand, suggests that the polypeptide clamp sites are dynamic and under allosteric control [17]. During translocation, the translocating chain binds protons with its acidic groups and forms an α helix inside the channel. The dynamic ϕ clamp site adjusts to accommodate the wider helix. The 2 Å per residue compression of the translocating chain from the extended-chain state to a helical one is proposed to allow for a power stroke to be created. Once helix propagates to the α clamp, an allosteric change in the structure of the ϕ clamp drives it to the clamped state. The clamped state of the ϕ clamp causes the peptide to convert from the helical state to the extended-chain state. This conversion of the peptide from helical to extended-chain conformation allows it to extend past the charge clamp and deprotonate down the gradient. The deprotonated peptide is then electrostatically committed to translocate by the charge clamp via the development of a repulsive event that prevents retrotranslocation. The cycle then repeats on the next segment of polypeptide until the rest of the protein is translocated. Here, to further distinguish between these two models, we investigate the dynamics of the ϕ-clamp interactions using a 10-residue guest–host peptide probe.

Results

Single-channel translocation reveals subconductance intermediates

A previously described guest–host peptide system of the generalized sequence, KKKKKXXSXX, was used [18]. The guest-residue sites, designated “X”, were substituted with Ala, Leu, Phe, Thr, Trp, or Tyr. Previously, we did not characterize the single-channel translocations of the guest–host peptide. Here, we use the peptide to probe the interactions at the ϕ-clamp site. A single PA channel was introduced into a planar bilayer, and 20 nM of one of the peptides was added to the *cis* side of the bilayer. In the initial characterization, the voltage membrane potential ($\Delta\psi$) was adjusted to 70 mV so that individual blockade events would correspond to translocations. (By definition, $\Delta\psi \equiv \psi_{cis} - \psi_{trans}$, where $\psi_{trans} \equiv 0$.) We observed four conductance states in these experiments for each of the guest–host peptides. The four states included a fully open-channel state (O), a fully blocked-channel state (B), and two intermediate conductance states (Fig. 1). One intermediate was a ~10% subconductance state (I_1), and the other intermediate was a ~50% subconductance state (I_2). During the translocation of the guest–host peptides with aromatic insertions (Phe, Trp, and Tyr), these peptides exhibited an oscillation between the I_2 and B, where the oscillation occurred for the longest durations with the Trp peptide (Fig. 1).

Stereochemical variants of the guest–host Trp peptide

To further probe the oscillation in the single-channel translocations of the guest–host peptide, we chose the Trp peptide to vary its stereochemistry. The Trp peptide was selected because it exhibited the longest oscillation events of the peptides tested. Also, in a prior study, it was shown that Trp containing sequences could expedite the translocation of a two-domain substrate [18]. Furthermore, this peptide would test the steric constraints of the PA channel, since it was sterically bulky. In addition to the natural peptide containing all L-

amino acids (L-Trp), we also synthesized the Trp peptide with all D-amino acids (D-Trp) and with an alternating pattern of D- and L-amino acids (D,L-Trp). While the L-Trp and D-Trp peptides could make right-handed and left-handed helices, respectively, the D,L-Trp peptide could not cooperatively form either handedness of a helix. Moreover, the D,L-Trp peptide should be the least sterically bulky on average since it can only populate extended-chain states.

Ensemble steady-state measurements were first taken for these stereochemical variants. In these experiments, an ensemble of multiple channels was inserted from the *cis* compartment. The applied $\Delta\psi$ was stepped from −20 to 110 mV at 5 mV increments, and the currents were recorded. Then, as the peptide concentration was raised in increments in the *cis* compartment, the $\Delta\psi$ range was again probed. The data were processed as individual steady-state binding curves (Fig. 2a). The concentration of 50% blockade or saturation ($K_D$app) could be determined from Hill model fits at each voltage. The Hill model (Fig. 2b) was chosen because it was previously found that the Trp peptide bound in a cooperative manner [18]. The overall shape of the $K_D$app *versus* $\Delta\psi$ plot was chevron- or V-shaped. There was a positively sloped arm at high positive $\Delta\psi$ that corresponded with translocation, and there was a negatively sloped arm at lower positive and negative $\Delta\psi$ that corresponded with retrotranslocation or dissociation back to the *cis* compartment. The L-Trp peptide translocated most efficiently, relative to the D-Trp and D,L-Trp peptides.

Single-channel translocation experiments were also performed using the stereochemical variants of the Trp peptide. For these experiments, a single channel was inserted into a planar bilayer from the *cis* compartment, and the substrate Trp peptide was added to the *cis* compartment. Individual closures and openings of the channel were recorded at a range of voltages spanning +10 to +110 mV (Fig. 3a–c). The dwell times for the closures of the channel including all intervening intermediates were processed by the cumulative distribution function (CDF; Fig. 3d). This distribution was representative of unblocking either by translocation or by retrotranslocation (dissociation). The CDF at each voltage tested was fit by a single-exponential function to get an observed rate constant (k_{obs}). The k_{obs} values obtained at each voltage were plotted against $\Delta\psi$ as $RT \ln k_{obs}$, where R is the gas constant and T is the temperature (Fig. 3e). These plots revealed a chevron-shaped trend, where the lower voltages sloped negatively, and the higher voltages sloped positively. Because the slopes correspond to the charges required to cross the limiting barrier, and the peptide is net positive +5 in charge, the negatively sloped arm of the chevron at low voltages corresponds to dissociation back to the *cis* side of the membrane, and the positively sloped arm of the chevron at higher voltages corresponds to translocation through the PA channel.

The arms of the chevrons for the three stereochemical variants were roughly parallel, meaning that the charge requirements for crossing the major rate-limiting barrier possessed roughly the same charge dependence for each peptide. The L-Trp peptide translocated the fastest relative to the D-Trp and D,L-Trp. D-Trp and D,L-Trp translocated ~10 fold slower than L-Trp. Interestingly, D-Trp dissociated to the *cis* side ~20 fold slower than L-Trp. These results suggest that stereochemistry does influence the translocation of peptides, and thus, the peptides do not simply form nonspecific extended-chain structures during translocation.

Subconductance intermediates are part of translocation pathway

During single-channel blockade events, the peptide may either be translocating productively or retrotranslocating/dissociating unproductively back to the *cis* compartment. To determine whether the subconductance intermediates were part of the translocation pathway rather than the dissociation pathway, we tested whether the appearance of the intermediates in single-channel experiments correlated with observations made in ensemble steady-state experiments for wild-type (WT) PA and PA R178A channels. The R178Amutation is in the α clamp site. The appearance of intermediates was quantified as the percentage of channel blockade events that populated intermediates. The voltage dependence of this percentage as a function of the applied potential was sigmoid (Fig. 4a and b). The midpoint voltage of each sigmoid was determined. We then plotted the sigmoid midpoint voltages against the voltage midpoints of the ensemble steady-state chevrons (Fig. 4c). The two voltage midpoints were well correlated. Thus, the subconductance intermediates are part of the translocation mechanism but not the dissociation mechanism.

ϕ clamp mutation alters the translocation mechanism

Translocation of the Trp peptide through the ϕ clamp mutant, PA F427A, was then analyzed from the data obtained from ensemble steady-state measurements and single-channel experiments. The goal was to determine if the ϕ clamp site was the location in the channel where intermediates were populated during translocation. Ensemble steady-state measurements of L-Trp peptide through PA F427A were carried out under similar conditions as that of WT PA. Comparison of the individual steady-state binding curves (Fig. 5a) and Hill plots (Fig. 5b) revealed a shift in the chevrons of PA F427A toward lower voltages. The positively sloped arm that is indicative of translocation appeared at lower positive $\Delta\psi$ (30 mV) as compared to that of WT PA (~50 mV). This indicated that the L-Trp peptide required less driving force and translocated more efficiently when the ϕ clamp was mutated.

Single-channel translocation experiments were also carried out on stereochemical variants of the Trp peptide through the PA F427A channel. Individual closures and openings of the channel were recorded at a range of voltages spanning −60 to +110 mV (Fig. 5c–e). As compared to WT PA, the traces of channel recordings showed additional intermediates, which were more pronounced at lower positive voltages (Fig. 5f), indicating that the translocation pathway was altered for the ϕ clamp mutant. Furthermore, the peptide rarely fully blocked the channel, but instead, it formed the 90% blocked state in most of the events.

The data obtained were analyzed and plotted in a manner similar to that of WT PA, to obtain chevron plots, where the positive voltages sloped positively while the negative voltages sloped negatively (Fig. 5g). Interestingly, the positively sloped arms of the chevrons for the three stereochemical variants overlapped, indicating that there was little difference in the translocation of the variants when the ϕ clamp was mutated. The only difference observed between the translocation of variants was in their rates of dissociation. The D-Trp peptide dissociated the fastest, while the L-Trp and D,L-Trp had similar rates, unlike WT PA where D-Trp dissociated the slowest and L-Trp dissociated the fastest. Voltages lower than those used for WT PA were used for recording channel openings and closures for PA F427A, since the dissociation arm did not appear until the voltage was significantly reduced. This meant

that the translocation of the Trp peptides occurred even at low positive voltages, while dissociation back to the *cis* side of the membrane occurred only at negative voltages. The correlation between the voltage-dependent appearance of oscillating intermediates in single-channel experiments (Fig. 5h) and the ensemble steady-state blockade voltage midpoints was also assessed. Interestingly, maximum intermediates were observed at lower positive voltages, and the frequency at which the intermediates populated the pathway decreased at higher voltages. At negative voltages, very few intermediates were observed. Thus, the PA F427A ϕ clamp mutation altered the translocation pathway.

Constrained-helix peptide tests the flexibility of ϕ clamp site

A constrained-helix version of the Trp peptide was synthesized. In the constrained version, two residues were linked covalently in the position of a hydrogen bond that is typically formed in an α helix (Fig. 6a) [19]. This covalent bond prenucleates helix into the peptide, and as a result, it exhibits CD signal consistent with a formed α helix (Fig. 6b). The covalent linkage is referred to as a hydrogen bond surrogate (HBS). A control unconstrained peptide was made containing an N-terminal acetylation and alanine residue at the third position in the peptide. The goal of this experiment was to test if a sterically bulky Trp peptide, when locked into a helix, could translocate efficiently through a WT channel. The constrained peptide and the control peptide were each added separately to a single WTPA channel over a range of voltages. Single-channel events were recorded for each peptide, and the events were analyzed as CDFs to determine their kinetics. It was found that while the control could readily translocate at moderate voltages (Fig. 6c), the stapled-helix version of the Trp peptide did not show translocation until significantly higher voltages were reached (>100 mV; Fig. 6c). This result indicated that the constrained α helix peptide was likely sterically hindered and less able to translocate, and helix formation was responsible for the observed defect. Therefore, it can be inferred that the translocation of the peptide through the WT PA channel does require unfolding or some conformational change and may follow the extended-chain model of translocation.

The ϕ clamp is a narrow arrangement of phenylalanine residues (Phe427) in the center of the channel, which is required for translocase function. A recent electron microscopy structure of the channel showed that the ϕ clamp has a ~6 Å opening and is quite narrow [14]. To test whether the steric hindrance observed with the HBS constrained-helix Trp peptide was the result of the interaction with the narrow ϕ clamp, we performed single-channel translocation experiments on PA F427A channels, which are mutated at the ϕ clamp site (Fig. 6d). It was found that the constrained-helix HBS peptide and the unconstrained control translocated efficiently at moderate voltages with identical voltage dependencies (Fig. 6c). Thus, the α helical Trp peptide experienced steric hindrance at the WT ϕ-clamp site.

The individual single-channel records were examined for the population of intermediates. In WT PA channels, the constrained-helix HBS Trp peptide did not populate the oscillating intermediates as often as the unconstrained control Trp peptide over the entire voltage range tested (Fig. 6e). This phenomenon suggested that the oscillating intermediates were due to a conformational change in the peptide, which was abrogated by the introduction of the HBS staple. In this model, the conformation precluded by the HBS constraint is likely a non-

helical, extended-chain state. The conformational change may have also involved the ϕ clamp site, since it is the site of conductance blockade. Thus, the intermediates may have been populated when the ϕ clamp oscillated between two different states depending on the conformation of the peptide. On the other hand, when the ϕ clamp was mutated, the HBS-Trp peptide once again populated the conductance-detected oscillating intermediates (Fig. 6d). This observation indicates that the ϕ clamp tightly regulates translocation in the WT PA channel, while the PA F427A obliterates this property of the WT PA channel and is easily able to accommodate the sterically bulky constrained-helix HBS Trp peptide.

Discussion

When the 10-residue guest–host peptide of sequence KKKKKXXSXX translocates, it populates four conductance states: a fully blocked channel, a 50% conducting channel, a 10% conducting channel, and a fully open channel (Fig. 1). There may be other kinetic states of the system, but these would have conductances identical to the four states seen, thereby masking their detection. A key question raised in these studies is what do these states mean molecularly? Based upon the rapid oscillation observed for the Trp peptide, it was suggested that the ϕ clamp oscillates with the peptide. Thus, the ϕ clamp is a dynamic site in the translocation path through the channel. Of course, other possibilities exist, such as the peptide moves rapidly between two different binding sites in the channel. These two binding sites may lie within the cap. In this model, the ϕ-clamp site remains static. We disfavor the model of the static ϕ clamp because of the rapid rate the peptide oscillates between states. Also, prior work has established that the ϕ clamp can dilate and populate a more conducting state [17]. Hence, the bistable change in clamp diameter may coincide with the observed bistable oscillation for the Trp peptide in its translocation records. Regardless of the exact molecular picture, it is clear that the peptide–clamp interactions can be highly dynamic.

How do the observed dynamics fit into the molecular mechanism of translocation? We found that the events containing conductance intermediates occurred more frequently at higher voltages (Fig. 4a and B), where translocation dominates retrograde dissociation in the kinetics. We interpreted this to mean that the intermediates were populated during translocation but not during dissociation. Also, the intermediates were populated nearer to the end of a typical translocation event (Fig. 3a–c). The order in which the intermediates were populated suggested that the intermediates were populated later in the mechanism, that is, when the peptide was committed to translocating rather than dissociating back to the *cis* side of the membrane. To determine how the ϕ clamp was involved in the mechanism, we mutated the site to F427A, and single-channel translocation events were recorded. With the ϕ-clamp mutant, the intermediates appeared nearer to the start of a translocation event (Fig. 5c–e). These results demonstrated that the ϕ-clamp site determined the translocation pathway and was responsible for the population of the conductance intermediates.

The PA F427A mutant did not populate the fully blocked state very frequently. Instead, the most-blocked state it formed was the 90% blocked state. This result mirrored a recent study by Schiffmiller and Finkelstein, which showed that the PA F427A mutant was leaky, and it also had trouble reaching the fully blocked state for a series of peptides attached to yellow

fluorescent protein [20]. The site of the leak was likely at the ϕ clamp in both the prior study and the present one. For the L-Trp translocation records obtained with the PA F427A channel, there also was a considerable population of a 50% blocked state (Fig. 5c). This state is consistent with a non-helical peptide bound at a dilated F427A ϕ-clamp site (Fig. 5e).

The HBS constrained helix, however, did not form appreciable subconductance intermediates. This result suggested that in order for the intermediates to be populated, the peptide had to transition to a non-helical state. The HBS helix of course populated the fully blocked state, which would be expected for the sterically bulky substrate's interaction with the ϕ-clamp. All other tested peptides including the unconstrained HBS control peptide and the L-Trp, D-Trp and D,L-Trp peptides exhibited the subconductance intermediates. Of these, peptides, D,L-Trp was the most interesting since it formed the subconductance intermediates, and it presumably cannot form helix. Again, this result suggested that the intermediates were populated as non-helical conformations, which likely included extended-chain states.

The kinetics of peptide translocation for the various configurations of the Trp peptide revealed several trends. The most optimal configuration of the peptide is L-Trp. It is not surprising, given that it is the native stereochemistry of proteins. It translocated 10-fold faster than D,L-Trp and D-Trp peptides and ~100-fold faster than the HBS stapled peptide. The slower translocation of D,L-Trp and D-Trp demonstrated there were specific stereochemistry requirements for efficient translocation, but these requirements were not overbearing and the channel was fairly adaptable to all three configurations. Perhaps more surprising was the fact that the HBS helix version of the Trp peptide translocated substantially slower than L-Trp and the unconstrained control peptide. This result suggested that the steric accommodation of the ϕ clamp dominated the translocation kinetics. However, it should be noted that the HBS helix did translocate, and the channel and ϕ clamp could sterically accommodate a prenucleated alpha helix. Since the known structure of the ϕ clamp site has a 6-Å-diameter opening, then it must be that the clamp opens to at least 12–15 Å to pass the prenucleated HBS Trp helix. That said, it is not surprising then that channels lacking a ϕ clamp (F427A) could easily translocate the HBS stapled peptide. Therefore, peptides locked in a helix or precluded from forming one (D,L-Trp) were defective in translocating, suggesting that the conformational flexibility found in typical protein sequence was required for the most efficient translocation.

Taken together, these data argue for key aspects of the helix-compression mechanism of translocation. First, the single-channel translocation events reveal the population of distinct subconductance intermediates. These intermediates support the model that the peptide–ϕ-clamp interaction is highly dynamic especially for a sterically bulky peptide such as the Trp peptide. The population of these intermediates was not restricted to the Trp peptide, as other guest–host sequences populated the two subconductance intermediates (Fig. 1). These data also argue that peptide conformational flexibility is required for efficient translocation. On one hand, the HBS peptide (which is locked in a helix) had significant trouble translocating, but on the other hand, the D,L-Trp peptide (which cannot form a helix) was also defective in translocating. Thus, presumably, the most optimal sequence configuration could dynamically access helical and non-helical conformations. In line with the helix compression model, the

translocating chain is expected to dynamically form both helix and extended chain at key points in the mechanism.

Materials and Methods

Peptides and proteins

Guest–host peptides were synthesized as previously described [18]. D-Trp and D,L-Trp peptides were synthesized and purified by Elim Biopharmaceuticals, Inc. The HBS Trp peptide and control Trp peptide were produced with solid-phase synthesis. The HBS linkage was introduced by a previously described method [21]. WT PA, PA R178A, and PA F427A oligomers were produced as previously described [4].

Planar lipid bilayer apparatus

Planar lipid bilayer currents were recorded with an Axopatch 200B amplifier and a Digidata 1440A acquisition system (Molecular Devices Corp., Sunnyvale, CA) [4,8]. Membranes were painted on a 50-μm aperture of a 1-mL white Delrin cup with 3% (wt/vol) 1,2-diphytanoyl-*sn*-glycero-3-phosphocholine (Avanti Polar Lipids) in *n*-decane. The *cis* (side to which the PA oligomer is added) and *trans* chambers were bathed generally in universal bilayer buffer (UBB): 10 mM oxalate, 10 mM phosphate, 1 mM EDTA, 10 mM Mes, and 100 mM potassium chloride (pH 5.6). Single-channel recordings were filtered at 400 Hz using a multisection Bessel filter and recorded at 800 Hz using PCLAMP10 software. When higher time resolution was required, recordings were made using 1000 Hz electronic filtering and recorded at 2000 Hz. Ensemble recordings were similarly made at 200 Hz with matched filtering at 100 Hz. By definition, $\Delta\psi \equiv \psi_{cis} - \psi_{trans}$ ($\psi_{trans} \equiv 0$ V).

Ensemble steady-state peptide binding analysis

A bilayer was formed in a 50-μm white Delrin cup bathed in symmetric UBB (pH 5.6). PA channels were inserted by adding 2 nM of PA oligomer to the *cis* chamber at 30 mV. Upon stabilization of the ensemble current at about 1000–2000 pA, the *cis* chamber was perfused to exchange with fresh UBB at pH 5.6. Peptide ligand (L) was added in small increments to the *cis* side of the membrane, and a range of voltages of −20 mV to 110 mV was stepped in 5-mV increments. At each voltage, fraction of open channels (θ_{obs}) *versus* [L] plots were fit to a linearized Hill model, $\log [\theta_{obs}/(1 - \theta_{obs})] = -\log K_D\text{app} - n \log [L]$, to obtain a concentration for half saturation, $K_D$app, and a Hill coefficient, n.

Single-channel analysis

The *cis* and *trans* chambers were bathed in UBB at pH 5.6. A single PA channel was inserted into a painted bilayer at a $\Delta\psi$ of 30 mV by adding ~2 pM of PA oligomer (freshly diluted from a 2-μM stock) to the *cis* side of the membrane [8]. Once a channel inserted into the membrane, the desired peptide was added to the *cis* side of the membrane at 20 to 100 nM concentration. Data were acquired by stepping the voltage over the targeted range, collecting recordings for 2–5 min at each voltage.

Average current levels, i, of the blocked state, two intermediates, and the open state of individual channels were determined using the histogram function and Gaussian fit in

CLAMPFIT software. Absolute conductance levels, γ, for the two intermediates and open state were determined by subtracting the blocked-state current, i_C, value and dividing it by the voltage: $\gamma = (i - i_C)/\Delta\psi$.

Individual translocation or dissociation events were manually inspected for whether they formed intermediates during a closure event. Fractions of events with intermediates were tabulated and plotted against voltage. The curve empirically yielded a sigmoid relationship. The voltage midpoint of the sigmoid was determined for each peptide-channel combination tested.

'Recordings were kinetically analyzed by capturing individual closure events as blocked-state dwell times (t_{obs}) using the event detector in the CLAMPFIT10 software. These t_{obs} values were analyzed by the CDF, that is, the probability, P, that t_{obs} is less than or equal to time, t, or $P(t_{obs} \leq t)$. CDFs were obtained for each set of blocked-state t_{obs} in ORIGIN9. The blocked-state CDF fit well to a single-exponential function, $P(t_{obs} \leq t) = 1 - \exp(-k_{obs}t)$. The observed rate constants (k_{obs}) for the blocked-state dwell times were plotted as $\Delta G‡ = RT \ln k_{obs}$ and fit to the chevron function:

$$\Delta G^{\ddagger}(\Delta\psi) = RT\ln[\exp((\Delta G^{\ddagger}_{\ddagger o1} + z_1 F\Delta\psi)/RT) + \exp((\Delta G^{\ddagger}_{\ddagger o2} + z_2 F\Delta\psi)/RT)]$$

$\Delta G‡_{o1}$ and $\Delta G‡_{o2}$ are the activation energies at 0 mV of the dissociation and translocation arms of the chevron. The z_1 and z_2 values are the charges required to cross the rate-limiting barriers for the dissociation and translocation arms of the chevron. F is Faraday's constant.

Acknowledgments

We would like to thank Nathan Hardenbrook for his helpful comments and criticisms. This work was supported by the National Institutes of Health, Institute for Allergy and Infectious Disease (NIAID) funding R01 AI077703. P.S.A. thanks the National Institutes of Health (R01GM073943) for financial support.

Abbreviations used

PA	protective antigen
LF	lethal factor
EF	edema factor
Δψ	membrane potential
α clamp	α helix binding clamp
ϕ clamp	phenylalanine clamp
CDF	cumulative distribution function
WT	wild-type
HBS	hydrogen bond surrogate
UBB	universal bilayer buffer

References

1. Collier RJ. Membrane translocation by anthrax toxin. Mol Asp Med. 2009; 30:413–422.
2. Feld GK, Brown MJ, Krantz BA. Ratcheting up protein translocation with anthrax toxin. Protein Sci. 2012; 21:606–624. [PubMed: 22374876]
3. Milne JC, Furlong D, Hanna PC, Wall JS, Collier RJ. Anthrax protective antigen forms oligomers during intoxication of mammalian cells. J Biol Chem. 1994; 269:20,607–20,612.
4. Kintzer AF, Thoren KL, Sterling HJ, Dong KC, Feld GK, Tang II, et al. The protective antigen component of anthrax toxin forms functional octameric complexes. J Mol Biol. 2009; 392:614–629. [PubMed: 19627991]
5. Feld GK, Thoren KL, Kintzer AF, Sterling HJ, Tang II, Greenberg SG, et al. Structural basis for the unfolding of anthrax lethal factor by protective antigen oligomers. Nat Struct Mol Biol. 2010; 17:1383–1390. [PubMed: 21037566]
6. Cunningham K, Lacy DB, Mogridge J, Collier RJ. Mapping the lethal factor and edema factor binding sites on oligomeric anthrax protective antigen. Proc Natl Acad Sci U S A. 2002; 99:7049–7053. [PubMed: 11997439]
7. Miller CJ, Elliott JL, Collier RJ. Anthrax protective antigen: prepore-to-pore conversion. Biochemistry. 1999; 38:10,432–10,441.
8. Thoren KL, Worden EJ, Yassif JM, Krantz BA. Lethal factor unfolding is the most force-dependent step of anthrax toxin translocation. Proc Natl Acad Sci U S A. 2009; 106:21,555–21,560.
9. Krantz BA, Trivedi AD, Cunningham K, Christensen KA, Collier RJ. Acid-induced unfolding of the amino-terminal domains of the lethal and edema factors of anthrax toxin. J Mol Biol. 2004; 344:739–756. [PubMed: 15533442]
10. Krantz BA, Finkelstein A, Collier RJ. Protein translocation through the anthrax toxin transmembrane pore is driven by a proton gradient. J Mol Biol. 2006; 355:968–979. [PubMed: 16343527]
11. Duesbery NS, Webb CP, Leppla SH, Gordon VM, Klimpel KR, Copeland TD, et al. Proteolytic inactivation of MAP-kinase-kinase by anthrax lethal factor. Science. 1998; 280:734–737. [PubMed: 9563949]
12. Leppla SH. Anthrax toxin edema factor: a bacterial adenylate cyclase that increases cyclic AMP concentrations of eukaryotic cells. Proc Natl Acad Sci U S A. 1982; 79:3162–3166. [PubMed: 6285339]
13. Krantz BA, Melnyk RA, Zhang S, Juris SJ, Lacy DB, Wu Z, et al. A phenylalanine clamp catalyzes protein translocation through the anthrax toxin pore. Science. 2005; 309:777–781. [PubMed: 16051798]
14. Jiang J, Pentelute BL, Collier RJ, Zhou ZH. Atomic structure of anthrax protective antigen pore elucidates toxin translocation. Nature. 2015; 521:545–549. [PubMed: 25778700]
15. Wynia-Smith SL, Brown MJ, Chirichella G, Kemalyan G, Krantz BA. Electrostatic ratchet in the protective antigen channel promotes anthrax toxin translocation. J Biol Chem. 2012; 287:43,753–43,764. [PubMed: 22105075]
16. Basilio D, Jennings-Antipov LD, Jakes KS, Finkelstein A. Trapping a translocating protein within the anthrax toxin channel: implications for the secondary structure of permeating proteins. J Gen Physiol. 2011; 137:343–356. [PubMed: 21402886]
17. Das D, Krantz BA. Peptide- and proton-driven allosteric clamps catalyze anthrax toxin translocation across membranes. Proc Natl Acad Sci U S A. 2016; 113:9611–9616. [PubMed: 27506790]
18. Colby JM, Krantz BA. Peptide probes reveal a hydrophobic steric ratchet in the anthrax toxin protective antigen translocase. J Mol Biol. 2015; 427:3598–3606. [PubMed: 26363343]
19. Patgiri A, Jochim AL, Arora PS. A hydrogen bond surrogate approach for stabilization of short peptide sequences in alpha-helical conformation. Acc Chem Res. 2008; 41:1289–1300. [PubMed: 18630933]
20. Schiffmiller A, Finkelstein A. Ion conductance of the stem of the anthrax toxin channel during lethal factor translocation. J Mol Biol. 2015; 427:1211–1223. [PubMed: 24996036]

21. Miller SE, Thomson PF, Arora PS. Synthesis of hydrogen-bond surrogate alpha-helices as inhibitors of protein–protein interactions. Curr Protoc Chem Biol. 2014; 6:101–116. [PubMed: 24903885]

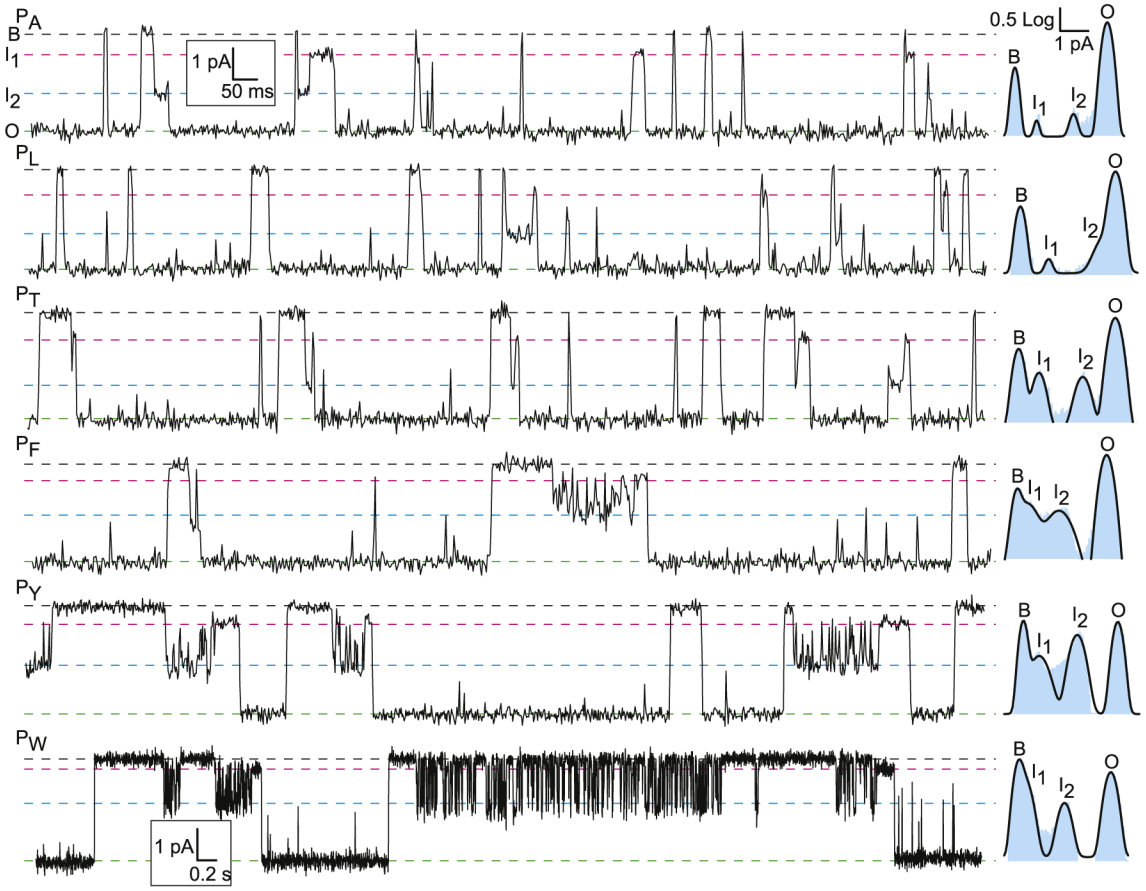

Fig. 1.

Single-channel translocation records of small guest–host peptide. Peptides, P_X, were of sequence KKKKKXXSXX, where X is a guest residue (A, L, T, F, Y, and W). The blocked (B), intermediate 1 (I_1), intermediate 2 (I_2), and open states (O) occur at characteristic levels for each guest–host peptide. The population of these states is given by the log-scale histograms on the right of each recording. Note that the timescale for the Trp peptide is unique to the other five peptides (which share their time and current scale bars).

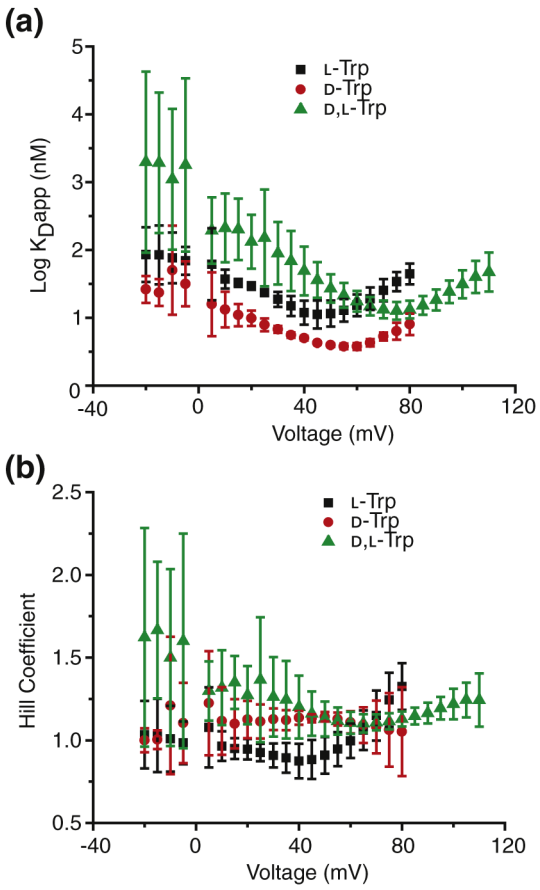

Fig. 2.

Ensemble steady-state measurements of stereochemical variants of Trp peptide. (a) The dissociation constants (log $K_D$app) from the ensemble steady-state measurements of L-Trp (black square), D-Trp (red circle), and D,L-Trp (blue triangle) for WT PA channels plotted against voltage. At each voltage, fraction of open channels (θ_{obs}) *versus* [*L*] plots were fit to a linearized Hill model, $\log [\theta_{obs}/(1 - \theta_{obs})] = - \log K_D\text{app} - n \log [L]$, to obtain a concentration for half saturation, $K_D$app, and a Hill coefficient, *n*. (b) Plot of Hill coefficients of L-Trp (black square), D-Trp (red circle), and D,L-Trp (blue triangle) against voltage.

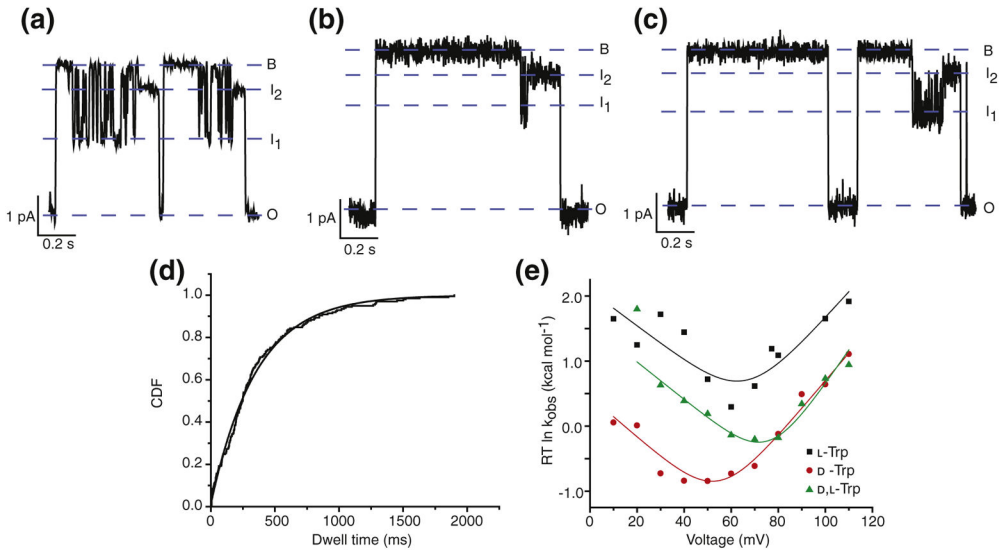

Fig. 3.

Single-channel measurements of stereochemical variants of Trp peptide. Single-channel planar lipid bilayer current records at 70 mV, symmetric pH 5.6 and 100 mM KCl of WT PA, following *cis*-side addition of (a) L-Trp (b) D-Trp, and (c) D,L-Trp peptides. Open (O), blocked (B), and intermediate (I1 and I2) states are indicated. Records are Gaussian-filtered to 50 Hz. (d) CDFs of closed-state dwell times (t_{obs}) fit to a single-exponential function defined in Materials and Methods. (e) Chevron plots of the observed rate constants (k_{obs}) for the blocked-state dwell times of WT PA in the presence of L-Trp (black), D-Trp (red), and D,L-Trp (green), plotted as $\Delta G‡ = RT \ln k_{obs}$ as a function of voltage. The data are fit to the chevron function defined in Materials and Methods.

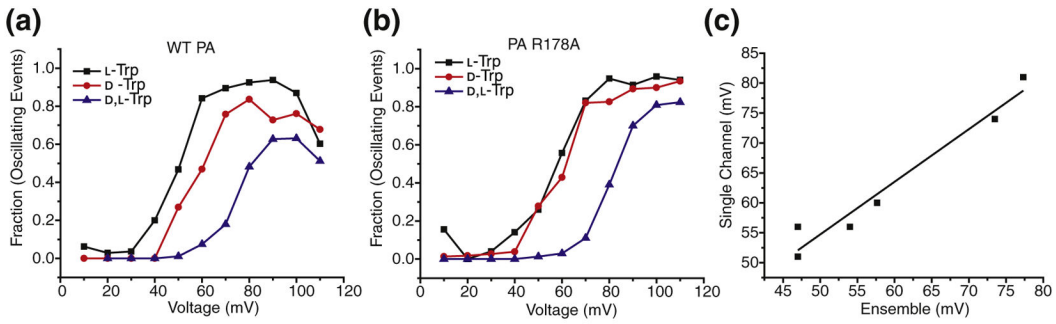

Fig. 4.

Intermediates are part of the translocation pathway. Plot of fraction of events with subconductance state(s) (oscillating events), against voltage (mV), in (a) WT PA channel in the presence of L-Trp (black square), D-Trp (red circle), and D,L-Trp (blue triangle) peptides; and (b) PA R178A channel in the presence of L-Trp (black square), D-Trp (red circle), and D,L-Trp (blue triangle) peptides. (c) Plot showing the correlation of voltages obtained from midpoint of sigmoid plots from single-channel measurements, and voltages at which maximum binding occurs in ensemble measurements. Adjusted R_2 value is 0.95.

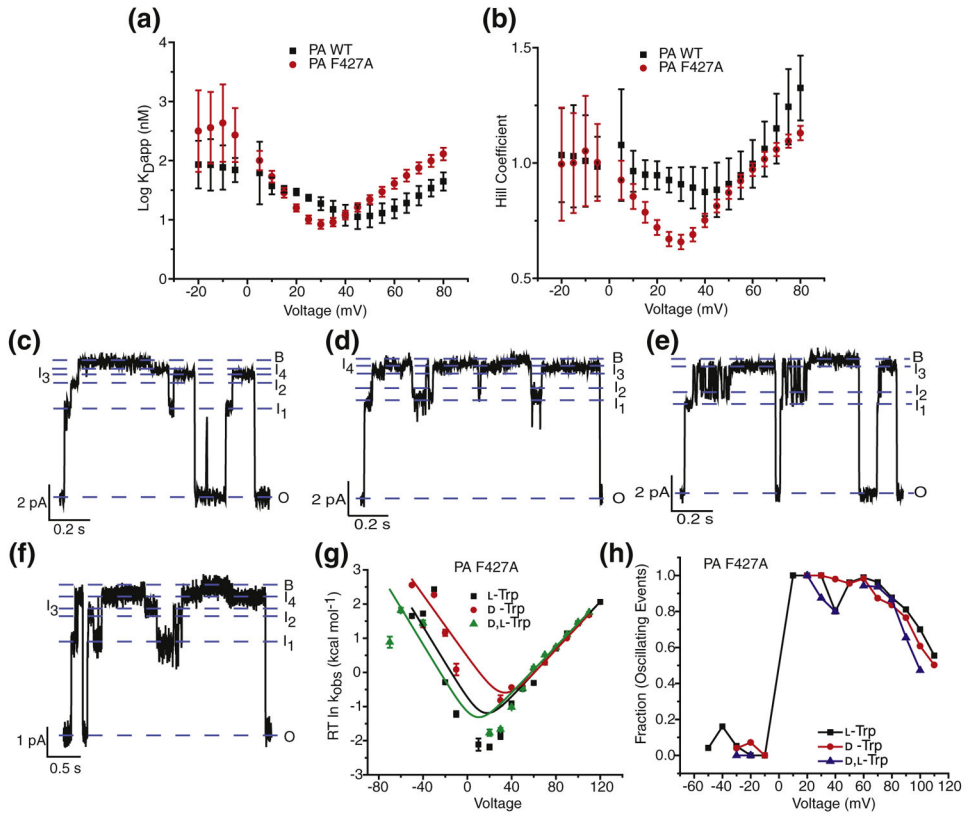

Fig. 5.

ϕ clamp mutation alters translocation mechanism. (a) The dissociation constants (log $K_D$app) from the ensemble steady-state measurements of L-Trp through WT PA channels (black) and PA F427A channels (red) plotted against voltage. (b) Plot of Hill coefficients of L-Trp through WT PA channels (black) and PA F427A channels (red) against voltage. Single-channel planar lipid bilayer current records at symmetric pH 5.6 and 100 mM KCl of PA F427A, following *cis*-side addition of (c) L-Trp (d) D-Trp and (e) D,L-Trp peptides at 70 mV, and (f) L-Trp at 50 mV. Open (O), blocked (B), and intermediate (I1 – I4) states are indicated. Records are Gaussian-filtered to 50 Hz. (g) Chevron plots of the observed rate constants (k_{obs}) for the blocked-state dwell times of PA F427A in the presence of L-Trp (black), D-Trp (red), and D,L-Trp (green) peptides, plotted as $\Delta G‡ = RT \ln k_{obs}$ as a function of voltage. The data are fit to the chevron function defined in Materials and Methods. (h) Plot of fraction of events with subconductance state(s) (oscillating events), against voltage (mV), in PA F427A channel in the presence of L-Trp (black), D-Trp (red), and D,L-Trp (blue) peptides.

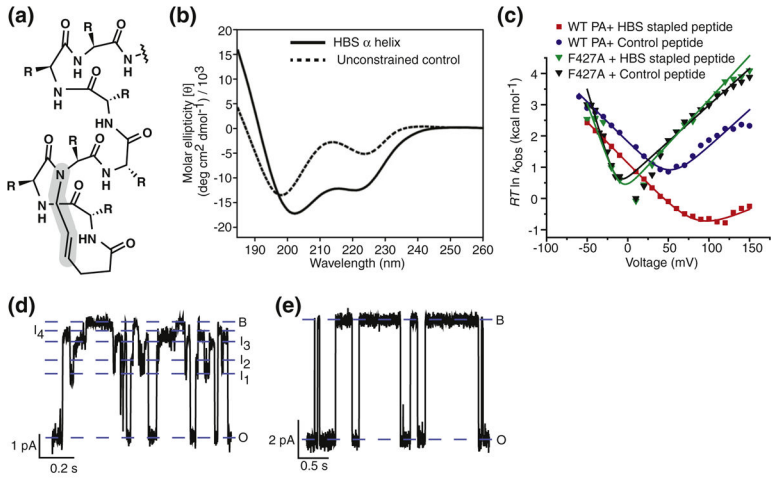

Fig. 6.

Constrained HBS α helix reveals the flexibility of ϕ clamp. (a) Structure of Trp peptide showing the HBS covalent linkage. (b) CD spectra showing that the HBS linkage effectively locks the peptide in an alpha helical conformation. Solid line represents the HBS α helix. Dashed line represents the unconstrained control peptide. (c) Chevron plots of the observed rate constants (k_{obs}) for the blocked-state dwell times of WT PA in the presence of HBS stapled peptide (red) and unconstrained control peptide (blue), and PA F427A in the presence of HBS helix (green) and unconstrained control peptide (black), plotted as $\Delta G^{\ddagger} = RT \ln k_{obs}$ as a function of voltage. The data are fit to the chevron function defined in Materials and Methods. Single-channel planar lipid bilayer current records at symmetric pH 5.6 and 100 mM KCl of (d) PA F427A, following *cis*-side addition of HBS stapled peptide at 50 mV, and (e) WT PA, following *cis*-side addition of HBS stapled peptide at 100 mV. Open (O), blocked (B), and intermediate (I_1–I_4) states are indicated. Records are Gaussian-filtered to 50 Hz.